GEO Belt Survey with WFCAM

Richard L. Kendrick, Matthew Bold
Lockheed Martin STAR Labs, 3251 Hanover Street, Palo Alto, CA, 94304, USA
Mike Irwin, Greg Madsen, Marco Riello
Institute of Astronomy, University of Cambridge
Cambridge, CB3 0HA UK
Tom Kerr, Watson Varricatt
Joint Astronomy Centre, 660 N. A'ohoku Place, Hilo, HI 96720, USA
Robert G. Mann, Nick Cross, Mike Read
Wide Field Astronomy Unit, Institute for Astronomy, University of Edinburgh, Royal Observatory Edinburgh, Edinburgh, EH9 3HJ UK

ABSTRACT

The United Kingdom Infrared Telescope (UKIRT) has been operating for 35 years on the summit of Mauna Kea as a premier infrared astronomical facility. In its 35th year the telescope will be turned over to a new operating group consisting of University of Arizona, University of Hawaii and Lockheed Martin. UKIRT will continue its astronomical mission with a portion of observing time dedicated to orbital debris and Near Earth Object detection and characterization assigned to NASA's Orbital Debris Program Office. During the past 10 years the UKIRT Wide Field Camera (WFCAM) has been performing large area astronomical surveys in J, H and K bands: One of the surveys (LAS) did it in YJHK bands. There were other surveys in the narrow band filter 2.122 micron H_2 and in the 1.644 micron FeII which observed large areas of the Galactic Plane. The data for these surveys have been reduced by the Cambridge Astronomical Survey Unit (CASU) in Cambridge, England and archived by the Wide Field Astronomy Unit (WFAU) in Edinburgh, Scotland. In early 2014 the Wide Field Camera (WFCAM) was used to scan through the GEO-stationary satellite belt detecting operational satellites as well as nearby debris. Accurate photometric and astrometric parameters have been developed by CASU for each of the detections and all data has been archived by WFAU. This paper will present the first results of these orbital debris surveys with WFCAM.

1. INTRODUCTION

In 2012 the United Kingdom Science and Technology Facilities Council (STFC) decided to discontinue funding for the operation of UKIRT, the 3.8 meter Infrared Telescope on Mauna Kea. The entire facility including all of the instrumentation will be handed over to the new operator by the end of 2014. The observatory is now directed with input from the University of Arizona Steward Observatory. The day to day operations are managed by the resident UKIRT staff and Lockheed Martin provides guidance for observations of earth orbiting objects. For the past several years UKIRT has been operating in a minimalist mode with a single instrument on the telescope to reduce costs. That instrument is the wide field survey instrument WFCAM. As a proof of principle WFCAM was used in the simplest mode to observe objects in GEO-synchronous orbit. This mode is a sidereal track mode where a target star is tracked through the night as it traverses the GEO Belt. Any GEO objects will appear as streaks in the image and by careful data reduction the position and photometric properties of the object can be determined. We decided to utilize the well refined world class WFCAM data pipeline that has been in operation for the past 10 years reducing all of the WFCAM data as well as other survey instrument data such as VISTA. In this paper we will describe the WFCAM instrument and data pipeline and we will present some of the initial GEO survey results.

2. WFCAM INSTRUMENT

An image of UKIRT taken inside the telescope dome is shown in Fig. 1. UKIRT is a traditional Cassegrain telescope that was completed in 1979. The yellow structure is the telescope support mount and the blue structure is the telescope. The long black cylinder is WFCAM.

Fig. 1. A view inside the UKIRT dome. The black cylindrical structure is WFCAM mounted to the front of the primary mirror cell. The primary mirror cover is closed. Photo by Paul Hirst, Joint Astronomy Centre.

WFCAM was designed and fabricated by the UK Astronomical Technology Center in Edinburgh Scotland. First light for the instrument at UKIRT was in 2004. The instrument is an innovative system that was designed for a large field of view. The large field of view requirement necessitated the mounting of the instrument between the primary and secondary mirrors due to the constraints of the initial telescope design which limited the available field behind the primary mirror at the traditional Cassegrain focus. Fig. 2 is a schematic of the WFCAM optical design.

The WFCAM instrument begins with the field lens shown in Fig. 2. This lens images the primary mirror onto a cold stop inside the WFCAM Cryostat. The next element is the window of the cryostat followed by a corrector plate that reduces any off axis wavefront aberrations. The next element is the tertiary mirror which brings the beam to a focus on the four HAWAII-2 detector arrays at the focal plane. Just in front of the detector arrays are a set of filters and field flatner elements. There is a set of Z, Y, J, H and K broad-band filters and two narrow-band filters (currently 1.644 micron [FeII] and 2.122 micron H2 1-0 S(1)filters) available. The detector arrays are maintained at approximately 75 degrees Kelvin and the other components in the cryostat are maintained at low temperatures around 100 degrees Kelvin depending on the element. An excellent description of the WFCAM instrument can be found in [1].

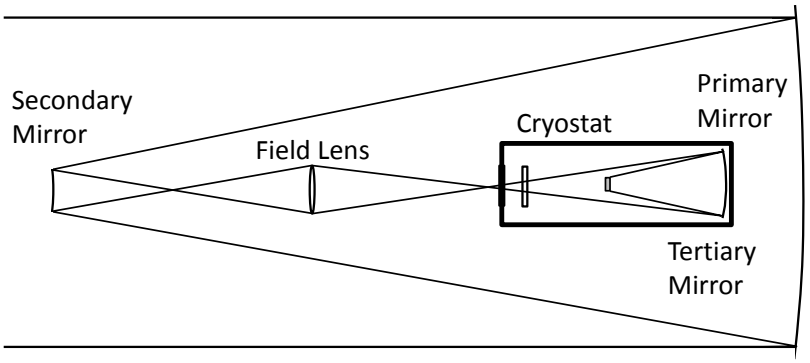

Fig. 2. The UKIRT-WFCAM optical schematic is shown. The WFCAM instrument begins with the field lens and includes all components in the cryostat.

Fig. 3. is a schematic of the WFCAM focal plane. There are four 2048 x 2048 pixel HAWAII-2 detector arrays with 18 micron pixel pitch. Each pixel is 0.4 arc-seconds on the sky. The detector arrays are arranged in a square paw print pattern.

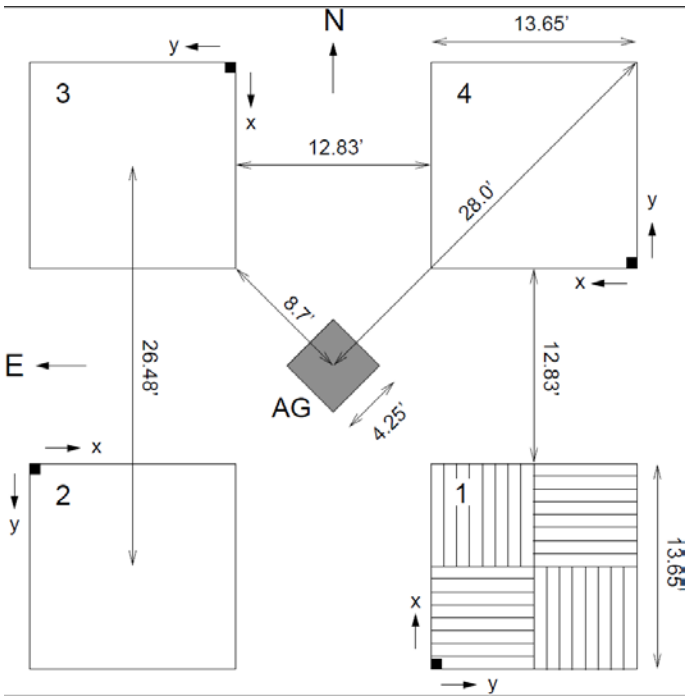

Fig. 3. The WFCAM focal plane layout is shown to scale.

The visible auto guider (AG) is positioned between the four HAWAII-2 sensor chips as shown in Fig. 3. The AG provides feedback to the secondary mirror which has a 100 Hz sample rate tip-tilt correction capability. In order to create a full 0.7 degree square image a set of four separate images are recorded with four separate telescope pointings to fill in the gaps between the HAWAII-2 detector arrays.

3. WFCAM DATA PIPELINE

The first stage of processing of WFCAM data for satellite analysis makes use of the standard VISTA Data Flow System (VDFS) which includes pipeline processing, database ingestion, production of enhanced database-driven products and dissemination via a purpose-built science archive. The VDFS is described in [2], [3] and [4].
All WFCAM science data are processed in Cambridge through a standard pipeline which makes use of master calibration images (darks, twilight flats) to help remove the gross instrumental 2D signatures. The image processing phase also includes corrections for non-linearity, reset anomaly, inter-pixel correlation, fringing, cross-talk and sky residual anomalies. All observations are processed through to the minimum schedulable block level which may involve interleaving (i.e., sub-pixel shifts), dithering and stacking. For each science image, a detected object catalogue is generated which is used for generating quality control information, and for both astrometric and photometric calibration with respect to 2MASS [5]. More than ten years of experience with WFCAM processing shows that we can readily achieve astrometric precision to better than 100mas and photometric calibration to better than 2% for normal, sidereally tracked images [6]. The standard WFCAM data processing flow is shown in Fig. 4. Processing steps specific to processing GEO orbit data are discussed in section 4. After processing the data is sent electronically to the Wide Field Astronomical Unit in Edinburgh. Here all of the image and catalogue data together with the related observational and processing metadata are archived in a searchable database. A good description of the WFCAM archive is given in [7].

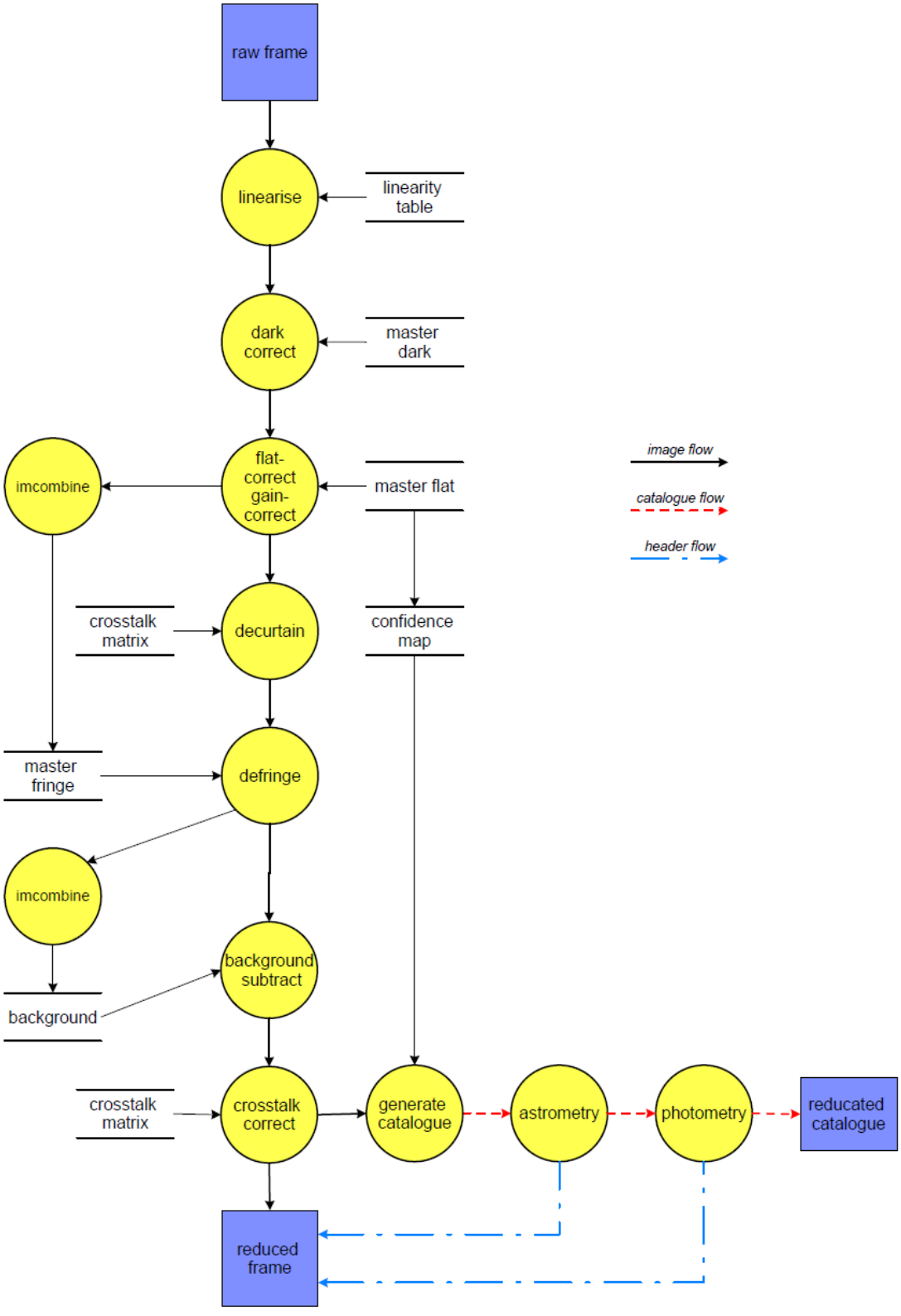

Fig. 4. The standard WFCAM Data reduction process is shown.

4. SIDEREAL TRACK DATA PROCESSING

The WFCAM images were taken with the telescope tracking at a sidereal or alternatively a non-sidereal rate. In this paper, we mainly discuss results from the sidereal track observations [8]. The normal pipeline science products described above in Section 3 cannot be used for satellite detection because the stacking procedure removes all traces of any satellites; the satellites appear as non-repeating, highly elongated streaks in single frames. However, the astrometric and photometric calibration information (i.e. WCS and magnitude zeropoint) remains valid.

After some experimentation it was clear that satellite detection on the individual images was not optimal (e.g. in 5 second exposures GEO-synchronous satellites produce a ~75 arcsecond east-west streak). We developed a new scheme to improve the detectability of the satellites by about 1.5 magnitudes and also to generate more reliable parameters for them. The main idea is to remove virtually all the background astronomical objects (unresolved stars and resolved galaxies) whilst leaving anything rapidly moving untouched, thereby retaining all the calibration information that is required for accurate astrometry and photometry. We achieve this through the following three steps:

1) identify isolated, contiguous, "circular" objects (or more specifically objects with ellipticity < 0.75) with a flux that exceeds the sky noise by 1-sigma; replace the pixel values of these objects with a local sky background value.

2) align the images and 'scrunch' them in the east-west (E-W) direction by a factor of 16; groups of 16 pixels in the E-W direction are replaced with the average value. Scrunching suppresses the presence of artefacts whilst improving the detectability of objects moving E-W (or nearly E-W).

3) create a catalog of detected objects on the scrunched images using conservative detection limits to ensure all moving objects are detected. The catalog records a number of parameters related to the position, size, shape, and brightness of satellite candidates.

This scheme is very successful in automatically identifying moving objects. However, it also selects a number of sources that are not real satellites. The most common sources of these false candidates are diffraction spikes and halos from bright stars, hot pixels, E-W grazing-incident cosmic rays, and cosmetic defects in the detector. We spent a considerable effort to identify and remove these false candidates while retaining true satellites. A number of diagnostic filters were implemented, e.g. objects appearing with high frequency at a particular right ascension and declination or detector position, shape parameters that are inconsistent with the majority of real satellites. A visual inspection of a large number of images confirm that this filtering reduces the frequency of false satellites in the catalog to below 1%. The major contributions to this very low level of contamination are scattered light artefacts and cross-talk images; these remain a future challenge to remove in an automated and robust way.

Fig. 5 shows representative images during the data processing steps. Fig. 5(a) is a raw J-Band image taken in sidereal scan mode with a 5 second integration time. Fig. 5(b) is after all the first stage pipeline processing has been applied. Fig. 5(c) shows the results after following step 1 described above where all astronomical objects are removed. This is a good example of the process and shows that there can be spurions from astronomical objects that in some way mimic GEO objects. In this case two stars happen to avoid deletion. These are removed during step 3 when appropriate detection limits are applied. There is a more problematic artefact that survives step 1 which is the dim streak to the right of the main GEO detection. This is a crosstalk artefact from the current HAWAII detector arrays. Work to identify and delete these artefacts is ongoing.

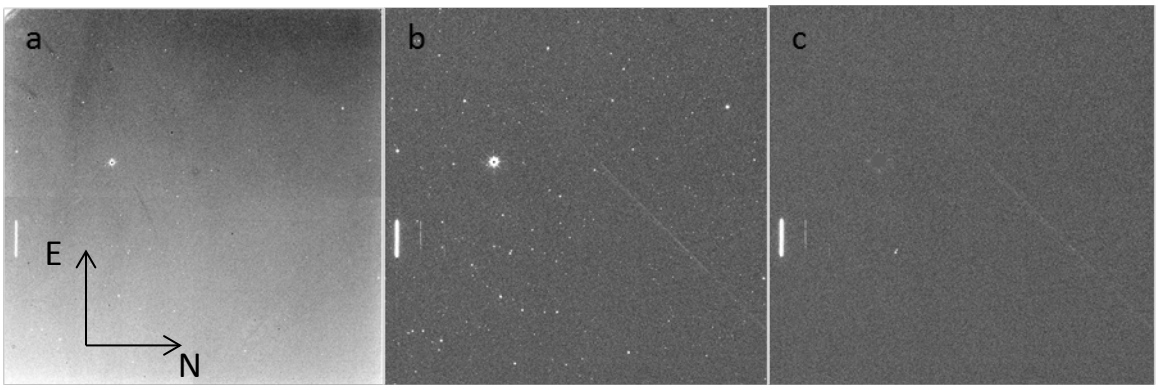

Fig. 5. The raw data is shown on the left and the product image is shown on the right.

Fig. 6 shows the result of following step 2 from above where the final image is scrunched by a factor of 16 in the East-West direction. Note that there are several remaining artefacts. One is the spurion created by the two closely spaced stars and the larger and more problematic is caused by a cross talk image.

Fig. 6 The scrunched image of Fig. 5c is shown. The effect of scrunching improves the detection limit by about 1.5 magnitudes. The GEO object is the large blob at the far left. Other artefacts can be seen that are filtered in step 3.

The scrunching process maintains the astrometric and photometric accuracies of the original image so that these smaller files can be used to extract the GEO object RA, DEC and magnitude. The final data reduction pipeline output is a text file that includes 20 some parameters including Hour Angle, Declination, Magnitude, Magnitude error, MJD and a variety of diagnostic parameters. For the January to May period we condensed 15 Terabytes of image data into a ~1 Megabyte text file.

5. RESULTS

A total of 54 nights of observing between 1 Jan - 20 May inclusive have been acquired and processed. The initial catalog (step 3) above generated 15,000 objects. This number was reduced to 7,243 after filtering. Fig. 7 shows several examples of various object types that are included in the data set. The majority of the detections are of the form shown in Fig. 5 with one or more 75 arc second streaks. The examples in Fig. 7 are not the norm but are very interesting.

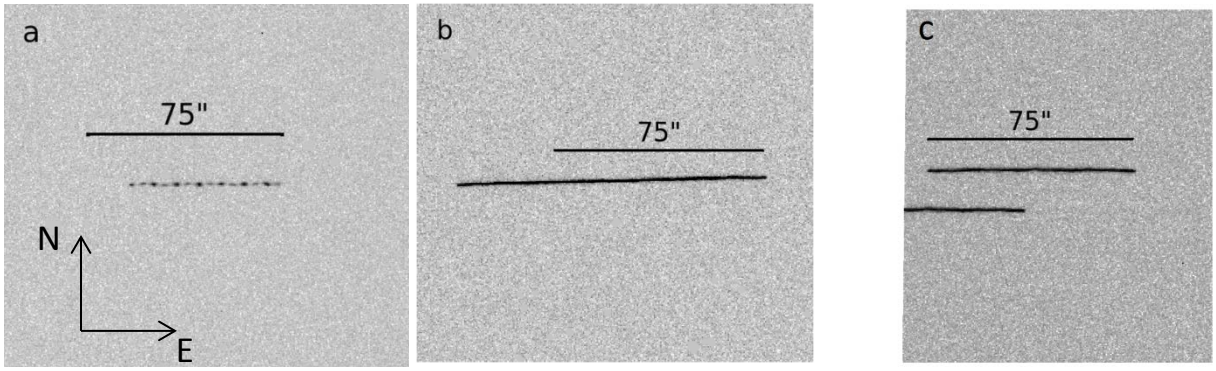

Fig. 7. Examples of various GEO-synchronous objects are shown. (a) an object with a temporal signature is shown. The period of the signature is approximately 0.8 seconds. The object is moving in the east west direction causing the foreshortening of the streak to 57". (b) is an object that is moving opposite the sidereal motion causing an elongation of the streak. This object is also moving slightly in the north-south or declination direction. (c) shows two objects that are relatively close together with one object falling off the edge of the detector.

Examples of various GEO-synchronous objects are shown in Fig. 7. In Fig. 7(a) a J-band processed image toward (HA,Dec) = (27.9, -3.1) observed in April 2014 is shown. The image is oriented with north as up and east to the left. The time-varying brightness is clearly seen; the peak-to-interpeak flux ratio is about 5. The average brightness over the 5 second exposure is 13.05 mag in J. The object is matched to satellite debris that is predicted to be 1.9' away from the center of this streak. Note that the streak length is significantly shorter than 75" expected for a GEO satellite implying that the object is moving somewhat in the sidereal direction.

In Fig. 7(b) a K-band processed image toward (HA,Dec) = (34.8, -3.4) taken in February 2014 is shown. This streak has a magnitude 10.17 in K and has moved ~ 2.4" to the south during the 5 second exposure. Note the streak length is significantly longer than the nominal GEO length implying that the object is moving somewhat in the anti-sidereal direction. The object is matched with satellite debris and is predicted to be 2.6' away from the center of this streak.

In Fig. 7(c) a K-band processed image toward (HA,Dec) =(-45.9, -3.4) observed in February 2014 is shown. There are two streaks on this image; the southernmost streak has fallen off the edge of the detector. The very bright full-length streak has a K-band magnitude 7.53. The objects are matched with station kept GEO satellites and are predicted to be 9.5" from the centre of the full-length streak and 10.8" away from the center of the shortened streak, assuming its full length is 75".

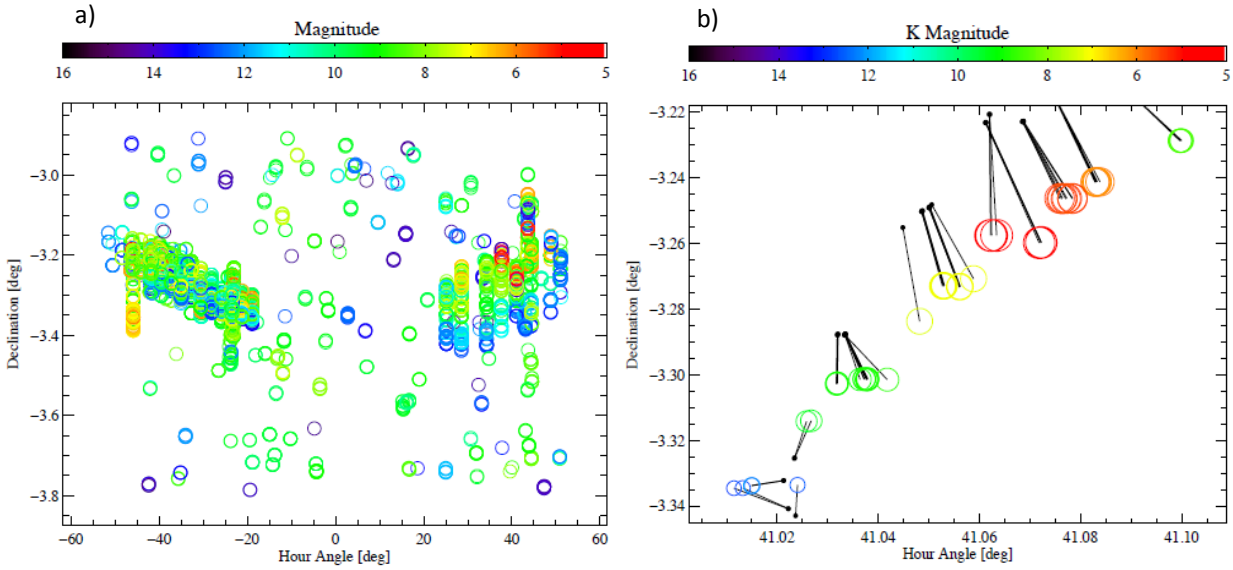

Fig. 8. a) All 7,243 objects detected are shown. b) one object and its predicted positions are shown with the black dots being the prediction and the colored circles being detections with size and color denoting magnitude.

In Fig. 8(a) A spatial distribution of 7,243 satellite candidates is plotted. The x and y axes are hour angle and declination, respectively. Each circle represents one detection; the color represents the object's magnitude as indicated in the color bar above the plot. Note that all three IR bands are overlayed here (J,H,K). Fig. 8(b) Shows the spatial distribution of 57 satellite candidates observed in K band. The x and y axes are hour angle and declination, respectively. Each colored, open circle represents one detection; the symbol size and color are proportional to its K-band magnitude. The solid black circles show the predicted location of the closest operational satellite at the time of each observation. One particular satellite is predicted to be the one closest to every observation in the figure. The satellite is a cable TV provider. A solid black line is drawn between the observed and predicted locations. On average, the predictions are offset by 1.5' from the observations. Note the very large change in brightness of this satellite (about 7 magnitudes) which is due to the variation of about 90 degrees in solar phase angle for these observations.

The hour angle and declination of our candidate list was compared with the predicted location of all known, man-made satellites. The orbital elements (TLEs) of ~15,000 satellites were obtained from space-track.org. For each satellite candidate, we select the full list of TLEs with epochs that are closest in time to 00:00 on the Julian date of

our observations (using a search window of ± 30 days). Note that this may be a significant source of error in the matching procedure; our observations may have been made after an orbital maneuver that is not incorporated into the TLE we are using. For example, the predicted locations of half of all GEOs vary by more than 30' (for the same satellite) when using TLEs with epochs between Jan-May 2014.

We propagate the orbits using the appropriate models. The propagation is based on a collection of open source code. To calculate the apparent position of satellites from UKIRT, we use the location parameters listed for the site.

We consider an observation to be 'matched' to a prediction if there is at least one satellite within a user-defined search radius. We find matches to 30% of our observations within a search radius of 30"; this percentage increases to 89% when using a 5' radius. Approximately 3% of our observations are matched to non-GEO satellites. Table 1 shows an ordered list of the name and frequency of the most commonly matched satellites. The difference between the predicted and observed locations may be used to refine the astrometry and timing of our observations.

Table 1. A list of detected objects and the total number of detections during the five month period are shown.

Common Name	**NORAD ID**	**# of Detections**
INTELSAT 18	37834	312
AMC-8	26639	287
TIANLIAN 1-02	37737	259
NSS 9	33749	257
GALAXY 14	28790	254
AMC-7	26495	253
EUTE 172A	28924	246
GALAXY 18	32951	244
GOES 15	36411	243
HORIZONS 1	27954	239
GALAXY 12	27715	238
AMC-10	28154	236
CIEL-2	33453	227
AMC-21	33275	226

One of the co-authors, Mike Irwin of CASU, suggested observing a satellite during the equinox period in K-Band to see if there is any evidence of a thermal signature as the satellite passed into the earth's shadow. Non-sidereal rate observations were performed on an operational satellite as it passed into the earth's shadow and the K-band magnitude was quantified as a function of time as shown in Fig. 9. This observation was performed with the telescope halted to maximize the detection capability. Fig. 9 shows the characteristic drop in intensity over a ~ 2 minute period as the sun passes behind the earth. Following this is a gradual decrease in signal that continues for approximately 4 minutes at which time the signal drops below the noise threshold. We plan to continue these sorts of measurements to determine the reason for this gradual decrease which may be refraction effects or some slight thermal signal from the satellites solar panels as they cool from around 100 degrees C to -150 degrees C.

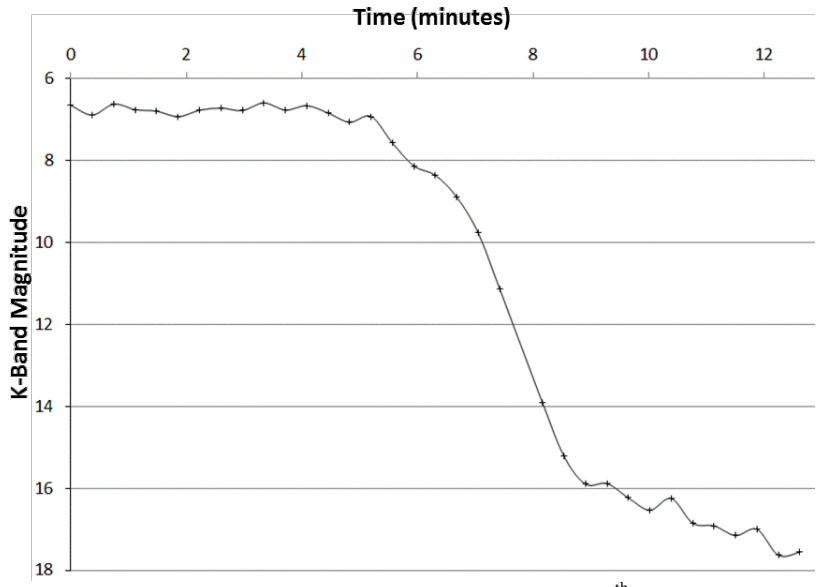

Fig. 9. The measured magnitude of an operational satellite is shown for March 18th 2014. The magnitudes are in K band from 2.03-2.37 microns.

6. ARCHIVED DATA AND ORBITAL DEBRIS ARCHEOLOGY

There is 10 years of WFCAM data that is archived at WFAU in Edinburgh Scotland. This data is available online in a searchable format. Many of the UKIRT astronomical surveys pass through areas of the sky that contain GEO objects. We have spent a modest amount of time searching through the publicly available data base and found that there are quite a few GEO objects in the WFCAM surveys. Fig. 10 is an example of a GEO object that was imaged during an astronomical survey. These streaks are usually an inconvenience to astronomers but we suggest that the WFCAM archive as well as all other astronomical archives contain a wealth of historical information on satellites and orbital debris that could be mined to create a historical record of the earth orbiting objects in the pursuit of what could referred to as orbital debris archeology.

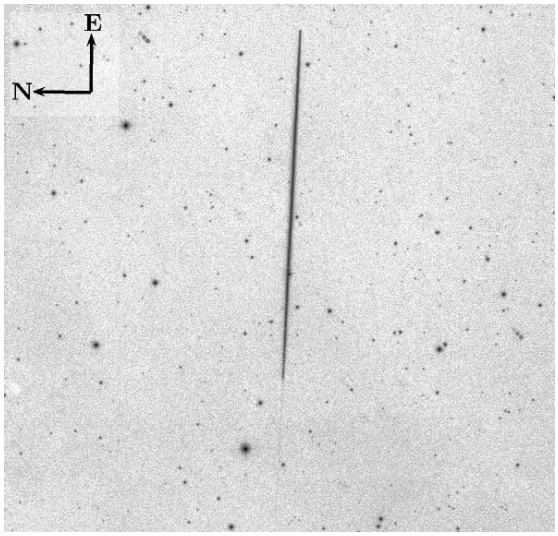

Fig. 10. J-band image of a GEO object using WFCAM on November 22, 2005.

7. SUMMARY

During the first five months of 2014 we demonstrated the utility of a premier astronomical telescope repurposed to observe orbital debris and satellites in GEO-synchronous orbit. While the observations to date have been rudimentary we believe that astronomical instruments such as WFCAM can provide an excellent orbital debris data base which will facilitate the characterization of orbital debris in the GEO belt. UKIRT will be moving to Cassegrain mode in August and September of 2014 in an effort to demonstrate the use of spectroscopic instruments in characterizing orbital debris.

8. ACKNOWLEDGEMENTS

The authors would like to thank Dr. Susan Lederer and Dr. James Frith of the NASA Johnson Space Center Orbital Debris Program Office for the support of this work and for their many helpful suggestions. The authors would also like to thank Gary Davis and the staff of the Joint Astronomy Center in Hilo, Hawaii for their help in the UKIRT transition.

9. REFERENCES

1. M. Casali, A. Adamson, C. Alves de Oliveira, O. Almaini, K. Burch, T. Chuter, J. Elliot, M. Folger,S. Foucaud, N. Hambly, M. Hastie, D. Henry, P. Hirst, M. Irwin, D. Ives, A. Lawrence, K. Laidlaw, D. Lee,J. Lewis, D. Lunney, S. McLay, D. Montgomery, A. Pickup, M. Read, N. Rees, I. Robson, K. Sekiguchi,"The UKIRT wide-field camera", *Astron. & Astrophys.* **467**, 777-784 (2007).
2. James P. Emerson, Mike J. Irwin, Jim Lewis, Simon Hodgkin, Dafydd Evans, Peter Bunclark, Richard McMahon, Nigel C. Hambly, Robert G. Mann, Ian Bond , Eckhard Sutorius , Michael Read , Peredur Williams, Andrew Lawrence, Malcolm Stewart, "VISTA data flow system: overview", *Proceedings of the SPIE*, Edited by Quinn, Peter J.; Bridger, Alan, **5493**, 401-410 (2004).
3. Mike J. Irwin, Jim Lewis, Simon Hodgkin, Peter Bunclark, Dafydd Evans, Richard McMahon, James P. Emerson, Malcolm Stewart, Steven Beard, "VISTA data flow system: pipeline processing for WFCAM and VISTA", *Proceedings of the SPIE*, Edited by Quinn, Peter J.;Bridger, Alan, **5493**, 411-422 (2004).
4. Nigel C. Hambly, Robert G. Mann, Ian Bond, Eckhard Sutorius, Michael Read, Peredur Williams, Andrew Lawrence, James P. Emerson, "VISTA data flow system survey access and curation: the WFCAM science archive", *Proceedings of the SPIE*, Edited by Quinn, Peter J.;Bridger, Alan**, 5493**,423-431 (2004).
5. M. F. Skrutskie, R. M. Cutri, R. Stiening, M. D. Weinberg, S. Schneider, J. M. Carpenter, C. Beichman, R. Capps, T. Chester, J. Elias, J. Huchra, J. Liebert, C. Lonsdale, D. G. Monet, S. Price, P. Seitzer, T. Jarrett, J. D. Kirkpatrick, J. E. Gizis, E. Howard, T. Evans, J. Fowler, L. Fullmer, R. Hurt, R. Light, E. L. Kopan, K. A. Marsh, H. L. McCallon, R. Tam, S. Van Dyk, and S. Wheelock, "The Two Micron All Sky Survey (2MASS)", *Astronomical Journal*, **131**, 1163 (2006).
6. S. T. Hodgkin, M. J. Irwin, P. C. Hewett and S. J. Warren, "The UKIRT wide field camera ZYJHK photometric system: calibration from 2MASS",*Monthly Notices of the Royal Astronomical Society*, **394**, 675-692 (2009).
7. N.C. Hambly, R.S. Collins, N.J.G. Cross, R.G. Mann, M.A. Read,E.T.W. Sutorius, I.A. Bond, J. Bryant, J.P. Emerson, A. Lawrence,J.M. Stewart, P.M. Williams, A. Adamson, S. Dye, P. Hirst and S.J. Warren, "The WFCAM Science Archive", *Monthly Notices of the Royal Astronomy Society*, **384,** 637-662 (2008).
8. S. M. Lederer, "NASA's Newest Orbital Debris Ground-based Telescope Assets: MCAT and UKIRT", AMOSTECH 2014.